Deep ocean sound speed characteristics passively derived from the ambient acoustic noise field

Evers, Läslo; Wapenaar, Kees; Heaney, KD; Snellen, Mirjam

DOI
10.1093/gji/ggx061

Publication date
2017

Document Version
Final published version

Published in
Geophysical Journal International

Geophysical Journal International

Geophys. J. Int. (2017) **210,** 27–33
Advance Access publication 2017 February 21
GJI Marine geosciences and applied geophysics

doi: 10.1093/gji/ggx061

Deep ocean sound speed characteristics passively derived from the ambient acoustic noise field

L.G. Evers,[1,2] K. Wapenaar,[2] K.D. Heaney[3] and M. Snellen[4]

[1] *Department of Seismology and Acoustics, Royal Netherlands Meteorological Institute,* 3731 *GA De Bilt, The Netherlands. E-mail: evers@knmi.nl*
[2] *Department of Geoscience and Engineering, Faculty of Civil Engineering and Geosciences, Delft University of Technology,* 2628 *CN Delft, The Netherlands*
[3] *Ocean Acoustical Services and Instrumentation Systems, Inc., Lexington, MA* 02421, *USA*
[4] *Department of Operations and Control, Faculty of Aerospace Engineering, Delft University of Technology,* 2629 *HS Delft, The Netherlands*

Accepted 2017 February 15. Received 2017 February 14; in original form 2016 October 5

SUMMARY

The propagation of acoustic waves in the ocean strongly depends on the temperature. Low-frequency acoustic waves can penetrate the ocean down to depths where few *in situ* measurements are available. It is therefore attractive to obtain a measure of the deep ocean temperature from acoustic waves. The latter is especially true if the ambient acoustic noise field can be used instead of deterministic transient signals. In this study the acoustic velocity, and hence the temperature, is derived in an interferometric approach from hydrophone array recordings. The arrays were separated by over 125 km, near Ascension Island in the Atlantic Ocean, at a depth of 850 m. Furthermore, the dispersive characteristics of the deep ocean sound channel are resolved based on the retrieved lag times for different modes. In addition, it is shown how the resolution of the interferometric approach can be increased by cross correlating array beams rather than recordings from single-sensor pairs. The observed acoustic lag times between the arrays corresponds well to modelled values, based on full-wave modelling through best-known oceanic models.

Key words: Atlantic Ocean; Interferometry; Acoustic properties; Wave propagation.

1 INTRODUCTION

From theoretical considerations it follows that the acoustic traveltime between two sensors can be obtained from the ambient noise field. In underwater acoustics, this traveltime strongly depends on the depth and temperature and to a lesser extent on salinity (Dushaw *et al.* 2009). In order to apply this theory in long range ocean acoustics and derive deep ocean temperature, hydroacoustic recordings from a station near Ascension Island are analysed. This station, called H10, is in place for the verification of the Comprehensive Nuclear-Test-Ban Treaty and as such part of the International Monitoring System (IMS). H10 consists of two hydrophone triplets which are placed in the Sound Fixing and Ranging (SOFAR) channel (Dahlman *et al.* 2009). The SOFAR channel is a low-velocity layer in the deep ocean, that is, the average channel axis depth is 1.5 km, which allows low-frequency sound to be detected over long ranges (Munk & Forbes 1989). The efficiency of the SOFAR channel for sound propagation has already been used in studies related to earthquakes (Evers *et al*. 2014; De Groot-Hedlin 2005; Guilbert *et al.* 2005), icebergs (Chapp *et al.* 2005; Talandier *et al.* 2006; Evers *et al.* 2013), explosions (Munk & Forbes 1989; Prior *et al.* 2011), marine mammals (Prior *et al.* 2012) and underwater volcanoes (Green *et al*. 2013). Guided wave propagation contributes to the limited acoustical attenuation by the SOFAR channel. In this study, the triplets are considered as arrays which are located to the north (7.84°S, 14.49°W) and south (8.95°S,14.65°W) of Ascension Island, at an inter-array distance of about 126 km, to avoid blocking by the island for sound coming from certain directions (see Fig. 1).

A study with deterministic transient signals from earthquakes has already shown the ability to probe the deep ocean's temperature with hydroacoustic recordings from the IMS (Evers & Snellen 2015). In this study, it is aimed to passively retrieve the deep ocean temperature from the ambient acoustic noise field. Sabra *et al.* (2012) successfully extracted the coherent ambient noise field between the hydrophones of an array, that is, a range of about 2 km. Brown *et al.* (2014) showed that the Green's function can be retrieved from the ambient noise field from sensors separated by 10 km in an coastal environment. Acoustic wave fronts have also been reconstructed from ambient noise measurements (Roux *et al.* 2004). Woolfe & Sabra (2015) positively tested the feasibility of the here used inter-array approach on the basis of signal-to-noise measures. Woolfe *et al.* (2015) showed how temperature variations at H10 can be retrieved from the ambient noise field on a monthly basis. Recently, Scholte waves were identified by applying interferometry to the H10 hydroacoustic data in the microseism-band, that is, around 0.2 Hz (Ball *et al.* 2016).

Here, a methodology will be presented of deriving the lag time from cross correlating the recorded ambient noise field from the northern and southern array of H10, with a resolution of an hour.

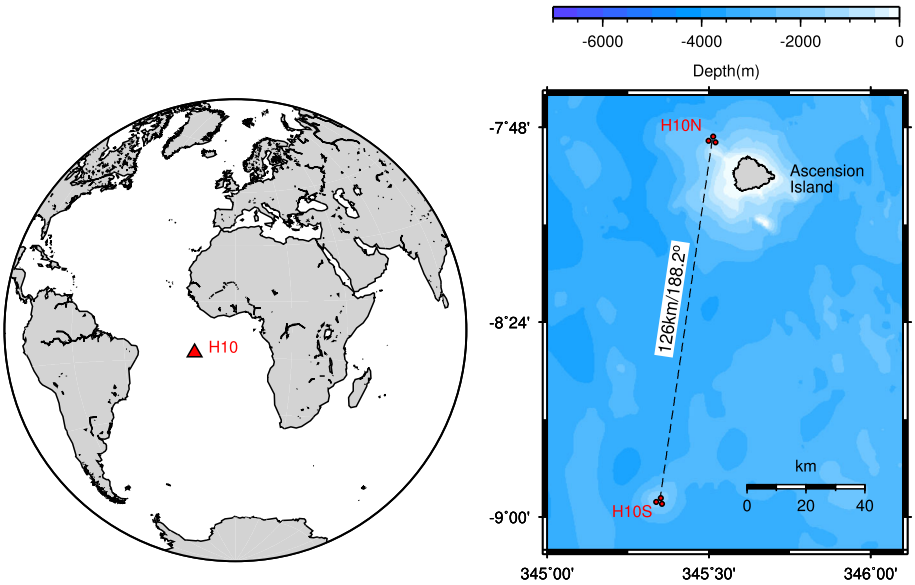

Figure 1. The location of H10 in the Atlantic Ocean near Ascension Island. H10 consists of two three-element hydrophone arrays, one to the north (H10N) and one to the south (H10S) of Ascension Island. The aperture of each array is about 2 km. The distance between the arrays is 126 km and the bearing connecting the two arrays is 188.2°.

In order to increase the signal-to-noise ratio (SNR) of this interferometric technique, array beams are cross correlated instead of single-sensor pairs. Furthermore, the dispersion of the SOFAR channel will be resolved on the basis of the proposed methodology, where different modes appear at different lag times. It will also be shown that these lag times, and hence the acoustic velocity, correspond well to values obtained from ocean acoustic modelling, based on temperature and salinity specification as a function of depth.

2 THEORY

Theory predicts that the correlation of passive noise recordings at two different sensors converges to the response that would be measured by one of the sensors if there were an active impulsive source at the position of the other. The main underlying assumption is that the ambient noise field is equipartitioned, that is, that the energy current is equal in all directions (Weaver & Lobkis 2001; Wapenaar 2003; Snieder 2004; Roux *et al.* 2004). Fortunately this strong assumption can be relaxed in many situations. For example, if only the direct wave between the two sensors is to be recovered, it is sufficient that the primary noise sources lie in a Fresnel zone around the extension of the ray that connects the two sensors, see, for example, fig. 2 in Snieder & Wapenaar (2010). In other words, it is sufficient that at least a part of the noise field propagates approximately along the ray that connects the sensors. Assuming this condition is fulfilled, the lag time between the sensors follows from the time-dependent cross correlation of the noise recordings at these sensors. With a known distance between the sensors, this lag time can be translated to the sound speed. The latter is parametrized as

$$c(z) = 1449.2 + 4.6T(z) - 0.055T(z)^2 + 0.00029T(z)^3 + .. \\ .. + (1.34 - 0.01T(z))(S(z) - 35) + 0.016z \quad (1)$$

with, $c(z)$ the sound speed in m s^{-1} as a function of depth z, $T(z)$ the depth-dependent temperature in centigrade, $S(z)$ the depth-dependent salinity in parts per thousand (Jensen *et al.* 2000).

3 CROSS CORRELATION RESULTS

Fig. 2 shows the results of cross correlating the recordings from hydrophones N2 (north) and S2 (south) over the period 2005 March 23 up to 2014 April 24. Cross correlations are calculated in one-hour time windows. This time window was found by trial and error, that is, both a shorter and longer time window reduced the absolute value of the cross correlation coefficient. The strength of the cross correlation depends on the coherency of the recordings at N2 and S2. It is expected that the coherency increases with decreasing frequency, because the attenuation due to scattering and absorption decreases. The SOFAR channel has a low-frequency cut-off of about 3 Hz, due to its limited thickness. Therefore, the recordings were pre-filtered with a second order Butterworth filter with corner frequencies of 3 and 5 Hz. Prior to filtering, the recordings are decimated with a factor of four from a sample rate of 250 to 62.5 Hz, which makes the computations more efficient. The cross correlation coefficients in Fig. 2 were averaged over 0.1 s lag time. A total of 74 617 hourly cross correlations were used, which is less than the total number of hours in the over nine years of data. Some hourly cross correlations were discarded because of gaps in the recordings. It follows from Fig. 2 that (1) the traveltime can indeed be resolved from the ambient acoustic noise field. The average peak in the cross correlation lies at a lag time of 85.5 s, which corresponds to a horizontal propagation velocity of 1477 m s^{-1} (the distance between N2 and S2 is 126.3 km). Only the positive lag times are resolved, since no clear persistent peak is found around -85.5 s. This means, with the chosen cross correlation setup, that the noise sources are concentrated to the south of H10. (2) There is also a strong cross correlation at a lag time of 0s in the recordings. For plotting purposes the maximum is not shown, but the correlation coefficient has an average value of 0.14 over the years. Furthermore, persistent cross correlations are found at lag times of -10 en 10 s. A close inspection of Fig. 2 also shows additional horizontal bands with high correlation coefficients at 20, 30, 40 and 50 s and the negative counterparts. Such a pattern can be caused by a repetitive source, like air gun signals from offshore seismic exploration surveys. Air guns provide repetitive acoustic signals. This might

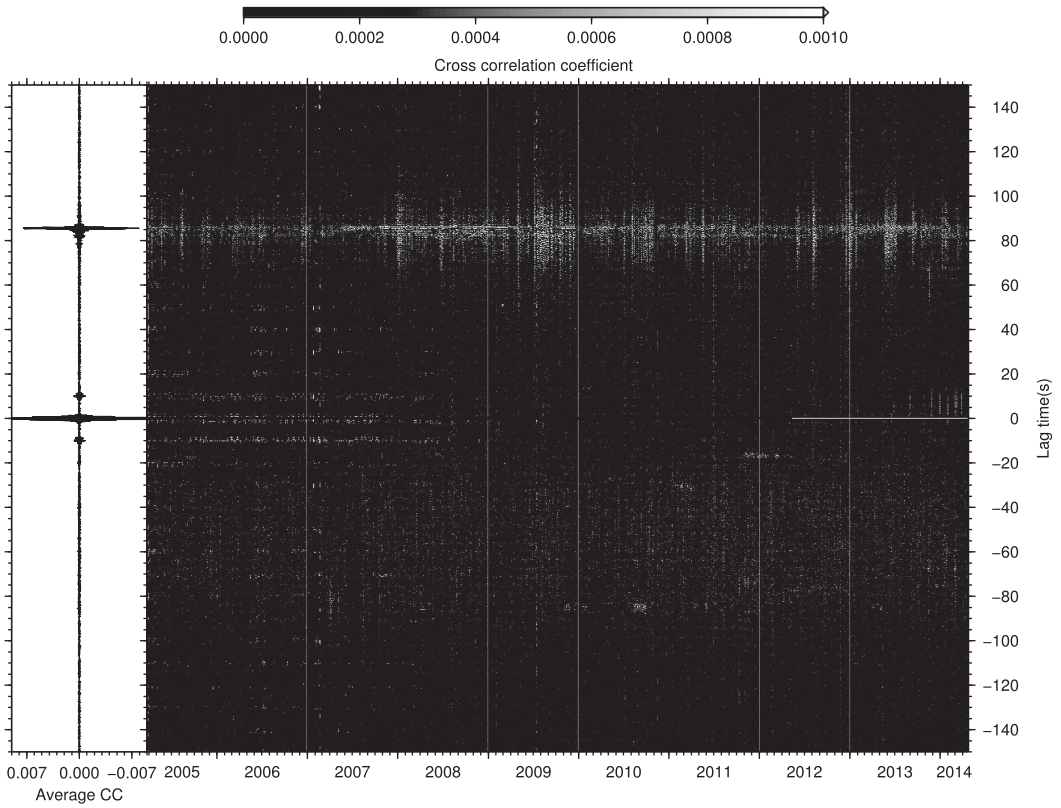

Figure 2. Hourly cross correlation results over the period 2005 March 23 up to 2014 April 24 using hydrophone N2 and S2. The data are bandpass filtered with a second-order Butterworth filter with corner frequencies of 3 and 5 Hz. Only the positive values of the cross correlation coefficients are shown to enhance the prominent features. The absolute values are averaged over a lag time of 0.1 s. A 1 hr time window is used for calculating the cross correlations. The frame to the left shows averaged cross correlation values over the years using 76 617 hourly cross correlation. The peak lies at a lag time of 85.5 s, other peaks are found around −10 and 10 s. The auto correlation has a value of 0.14 (not shown for plotting purposes).

explain why these sources show up at multiple lag times, since the cross terms in the cross correlation are also resolved. In other words, one waveform at one sensor will positively cross correlate with several waveforms of the other sensor. However, this does not explain the strong cross correlation at a lag time of 0 s. If the latter were to be explained by air gun signals, the source has to be at an equal distance from both hydrophone N2 and S2. It seems rather unlikely that this is the case, certainly for a period of over three and a half years, that is, up to halfway 2008 where high coefficients are retrieved.

Supporting Information Fig. S1 shows the cross correlation coefficients as a function of time for a lag time of 0 s. High coefficients are obtained from 2005 through 2007 after which the effect seems to reduce. By the end of 2009, the peaks of high valued coefficients have disappeared. Based on this observation, it is hypothesized that the phenomenon is caused by something electronic rather than acoustic signals or noise. A similar electronic disturbance on both hydrophones or in the data acquisition system can explain the high coefficients at a lag time of 0s, the 10+s multiples and its disappearance over time, due to possible changes in the system. Takagi *et al*. (2015) also found such a repetitive pattern of coherent cross correlations and attributed these to data logger noise. In the following sections, the peak at a lag time of 85.5 s will be further analysed; the results will not be affected by the unexplained high cross correlations coefficients at 0s and its multiples.

4 FREQUENCY DEPENDENCE

The coherency of the noise between hydrophone N2 and S2 is a function of frequency. In order to analyse up to which frequency coherency is available, a day of high cross correlation coefficients is further analysed. Fig. 3 shows the cross correlation results for a frequency of 0.5–15 Hz for 2011 May 5 between 11 and 12 h UTC. The raw unfiltered recordings of N2 and S2 are also shown. It has been tested that this arbitrarily chosen day and hour are representative. The envelopes are calculated to accurately measure the peak of the cross correlation. It follows from Fig. 3 that cross correlations for this day have coefficients up to 0.4. Significant cross correlation coefficients start to be retrieved from a frequency of 3 Hz and higher, which corresponds to the frequencies which the SOFAR channel can facilitate due to its limited thickness. Patches of energy in specific frequency bands appear more correlated than those in other frequency bands, which is typical for the modal propagation in the SOFAR channel (De Groot-Hedlin *et al.* 2009). As expected, the width of the envelope reduces with increasing frequency, enabling a higher time resolution. Furthermore, the lag time becomes smaller with increasing frequency. This can be understood by taking into account the shape of the SOFAR channel, where the lowest sound speed is at the channel axis. The smaller the wavenumber, the more the horizontal propagation energy is confined to the channel axis, which results in the larger lag times. As the frequency increases, more of the energy gets guided by the higher sound speeds surrounding the channel axis. In a ray-theoretical approach, the latter

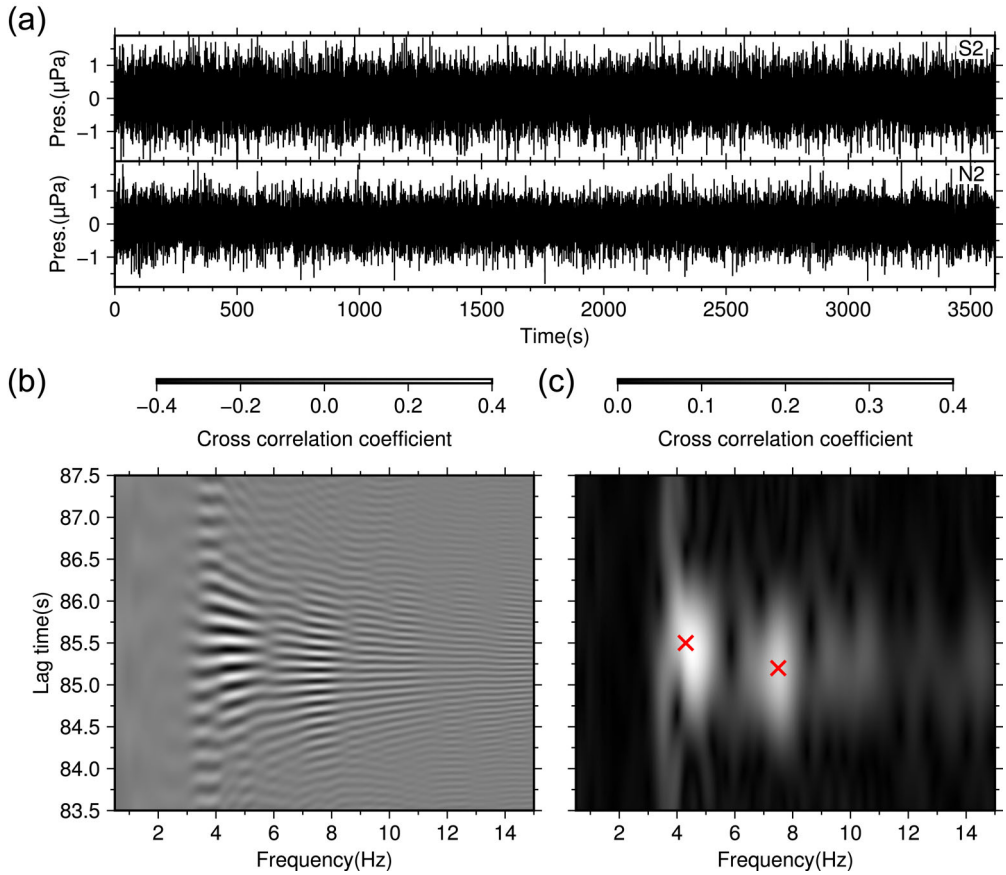

Figure 3. Cross correlation results as a function of frequency for 2011 May 5 between 11 and 12 hr UTC. (a) The hour of recordings at N2 and S2 are shown as unfiltered data. The cross correlation coefficients are shown for both (b) the cross correlation and (c) the envelop surrounding the cross correlation. These results are obtained with frequency bands of 1.0 Hz and a sliding window with steps of 0.1 Hz. The maxima (red crosses) are determined as 85.5 s at 4.3 Hz and 85.2 s at 7.5 Hz.

corresponds to rays being less horizontally incident on the receivers with increasing frequency. In this specific example, the difference in the lag time is 0.3 s, that is, 85.5 s at 4.3 Hz and 85.2 s at 7.5 Hz.

Following the above found dispersion, the whole data set is cross correlated for frequency bands of 3–5 Hz and 5–10 Hz.

For this purpose, a second order Butterworth filter is applied to the recordings prior to cross correlating. Decimation with a factor of four is again applied to the sample rate to reduce the computation time. Fig. 4 shows the results for these cross correlation computations, in the (a) low- and (c) high-frequency bands. For each hour of cross correlations, the envelopes are calculated, which are then averaged per month. The latter is done to make the picture less noisy and to only show the main variations. Only those hours are used for which the absolute value of the cross correlation coefficient is larger than 0.1, around the expected lag time. The average envelopes to the left of the main frames have peaks at 85.5 s (1477 m s^{-1}) for the 3–5 Hz band and 85.3 s (1481 m s^{-1}) for the 5–10 Hz band over the 9 yr period.

In an attempt to increase the SNR of the image by illuminating it with more acoustic daylight (Rickett & Claerbout 1999) beamforming is applied to the northern and southern array, which both consist of three hydrophones. Nakata *et al*. (2016) used a similar technique, the so-called double beamforming, to create a source and receiver array. As such, Nakata *et al*. (2016) were able to concentrate on specific bearings and slownesses in order to separate the incoming wave field. Here, the interferometric technique is most sensitive to the ambient noise along the axis between the two arrays. This also follows from the lag time obtained from the cross correlation of N2–S2. Positive values for the lag time imply that the noise sources are located to the south. Therefore, the beamforming is applied for a bearing of 188.2°, along the axis. The beamforming velocity is chosen as 1481 m s^{-1}, which follows from the analysis of over 4000 earthquakes recordings at the northern and southern array (see Supporting Information Fig. S2). For each day a beam is calculated by time delaying and summing the individual recordings. The beams are then cross correlated for each hour, following the same procedure as for the N2-S2 analysis. Prior to beamforming, the individual recordings are bandpass filtered with a second order Butterworth filter, with corner frequencies of 3–5 Hz (see Fig. 4b) and 5–10 Hz (see Fig. 4d). The beams are calculated with respect to N1 and S1, that is, a distance of 122.6 km. The lag times are 82.9 s (1479 m s^{-1}) for the low and 82.7 s (1482 m s^{-1}) for the high frequency band. The sound speeds retrieved from the lag times differ from the beamforming velocity. This is expected, as the beamforming velocity at each array is an estimate of the local sound speed, while retrieved sound speeds from the lag times are the averaged velocities over a distance of 126 km. No results are shown from 2013 October 21 and onwards, since hydrophone S1 stopped providing data. The difference in the lag times obtained from cross correlating the beams and hydrophone pair N2–S2 is due to the difference in distance, that is, 122.6 versus 126.3 km respectively.

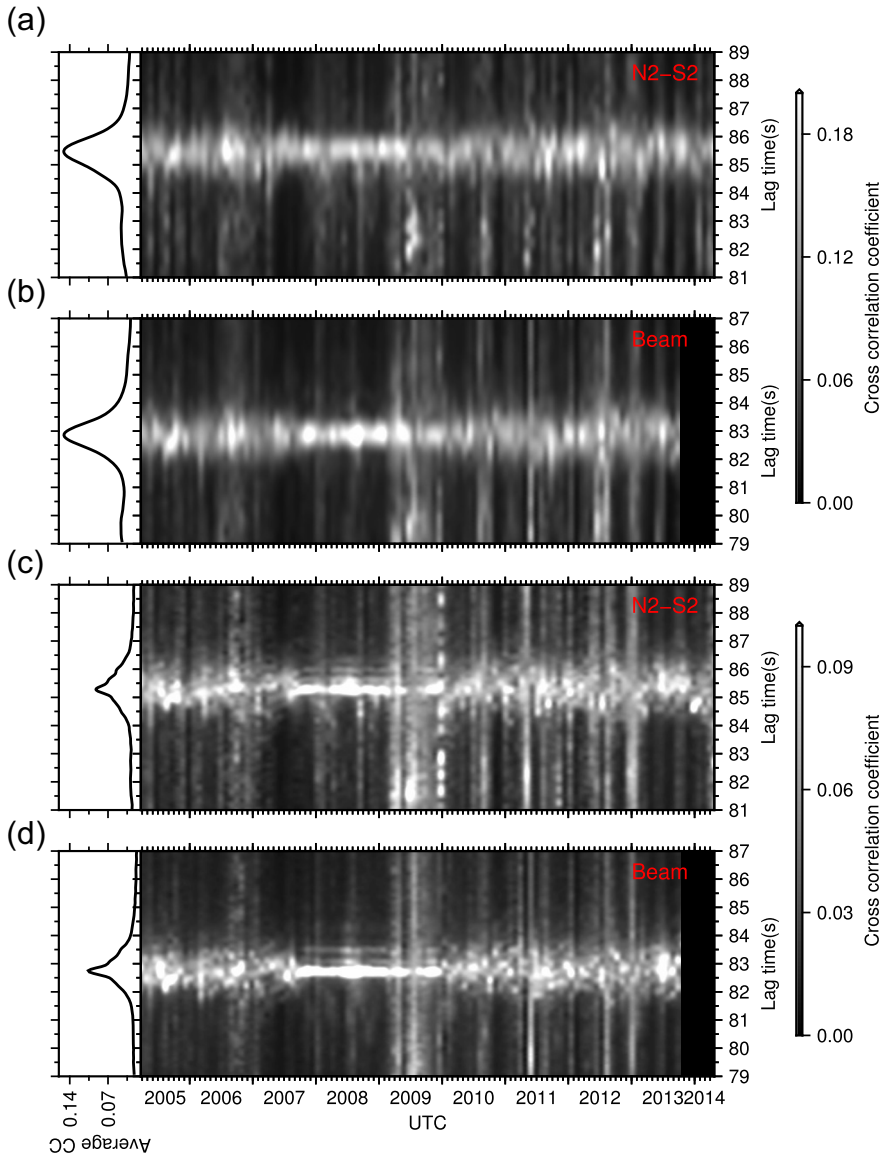

Figure 4. Cross correlation results as a function of frequency for a pass band (a) 3–5 Hz and (c) 5–10 Hz for the N2–S2 pair, at 126.3 km distance, and the associated beam (b,d). The beams are calculated with respect to hydrophone N1 and S1 at 122.6 km distance. The envelopes of the cross correlations are shown, which are calculated each hour. These envelopes are then averaged per month and over lag time intervals of 0.01 s. The frames to the left of the main frames show the average envelope over the whole time period of about 9 yr. The maxima are found as (a) 85.5 s for the 3–5 Hz band, (b) 82.9 s for the beam, and (c) 85.3 s for the 5–10 Hz band, (d) 82.7 s for the beam.

5 DISCUSSION AND CONCLUSIONS

It has been shown that the lag time between two hydrophones, at a depth of 850 m and separated by 126 km near Ascension Island, can be retrieved from the hourly cross correlations of the ambient acoustic noise field. This was also shown by Woolfe *et al.* (2015) on a monthly basis. A dispersive noise field was found where energy in the 3–5 Hz band travelled 0.2 s slower than that in the 5–10 Hz band. The latter is caused by the shape of the low velocity sound channel, that is, the SOFAR channel, where the smallest wavenumbers are most confined the channel axis.

In a next step, beamforming was applied to the three hydrophones of each array, to increase the SNR by illuminating the ocean with more acoustic daylight. The beams were formed along the axis between the northern and southern array, that is, towards the south. The beams were then cross correlated. The increase in SNR is mainly visible in the high-frequency band (see Fig. 5). A possible explanation can be found in the sharpness of the beam, which increases with increasing frequency. A sharper beam will result in a smaller variance of the retrieved lag times. This effect can be seen in Fig. 5, where the width of the average cross correlation peak reduces and its maximum increases. The increase is from 0.09 to 0.11 in the absolute value of the cross correlation. This increase is less than a factor $\sqrt{3}$, which one would expect from three instruments, meaning that the noise is not fully uncorrelated. The increase in the SNR is a function of the number of instruments. In general, it can be stated that the more instruments are deployed, the higher the increase in SNR will be. The positive effects of beamforming on the SNR are the clearest during 2008 and 2009 (see Figs 4b and d).

The propagation between the northern and southern array is modelled with a parabolic equation method (Collins 1993). The

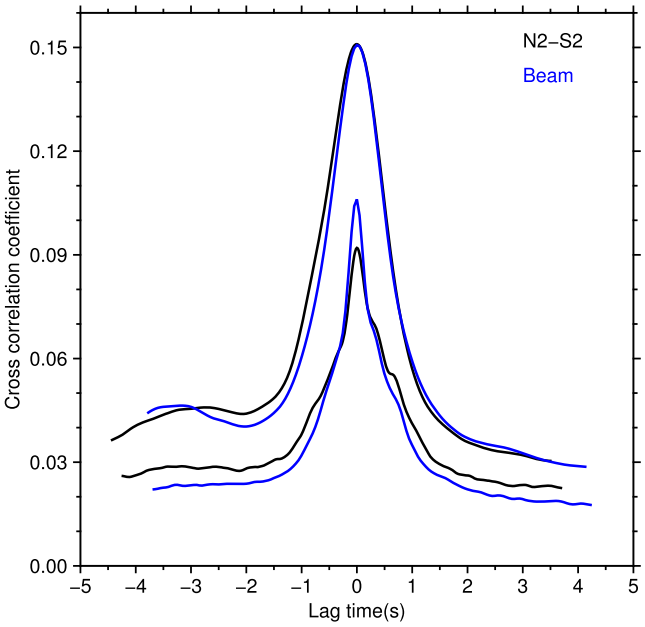

Figure 5. The average cross correlation envelopes calculated over all years. Shown are the results for cross correlating the beams (blue) of H10S and H10N and the results of the hydrophone pair N2–S2 (black). Both the results for the low-frequency (3–5 Hz, upper two curves) and high-frequency bands (5–10 Hz, lower two curves) are shown.

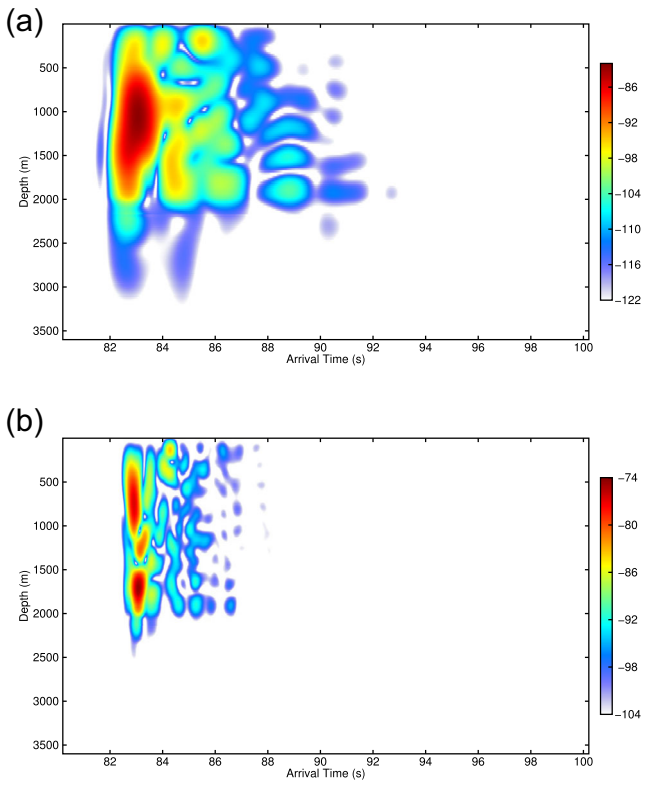

Figure 6. The traveltime between N1 and S1 obtained from modelling with the parabolic equation. Results are shown for (a) the low-frequency band of 3–5 Hz and (b) the high–frequency band of 5–10 Hz.

temperature and salinity, as a function of depth, are taken from the World Ocean Atlas (WOA09; Locarnini *et al.* 2010). Fig. 6 shows the results for the propagation between N1 and S1, which were also used as reference stations for the beamforming. The cross correlation procedure provided lag times of 82.9 s for the low and 82.7 s for the high frequency band. As follows from Fig. 6 similar values are obtained from the ocean acoustic modelling. The temperature at the axis of the channel, around 850m depth, is 5 °C in the WOA09. Differences between the seasons are negligible at the latitude of H10.

The question arises what the error is on the retrieved lag times and hence the 0.2 s due to dispersion? First, errors can arise in the acquisition by the moored hydrophones and due to propagation related issues. Under the influence of deep-ocean currents, the hydrophones can deviate from the vertical positions of their moorings. In this study, we also assumed propagation along the direct path, that is, the shortest distance. However, horizontal refractions due to inhomogeneities may lead to deviations of this shortest distance. Li & Gavrilov (2009) estimated an error in the back azimuth of 0.4°, consisting of 0.2° due to the movement and 0.2° caused by horizontal refraction. These estimates were also used by Evers *et al.* (2013) and Green *et al.* (2013) for error assessments. Using the interferometric approach, one of the sensors (or arrays if beamforming is used) becomes a source for the other. The back azimuth deviation of 0.4° translates to 3m over 126 km (or 0.002 s at 1481 m s^{-1}). Second, the lag time can be picked with a certain accuracy. We estimate that we can retrieve the lag time with an accuracy of a tenth of a wavelength of the cross correlation function. At the low-frequency end of 3 Hz this translates to 0.03 s and at the high of 15 Hz to 0.007 s. The accuracy of the pick is also dependent on the SNR; the associated error is more difficult to estimate. By selecting only hours with a cross correlation coefficient larger than 0.1, it was attempted to minimize such errors at low SNRs. Third, errors can also arise from the persistent sources outside the Fresnel zone or a non-homogeneous illumination of the hydrophones. Such cases would lead to smaller lag times. Here, it was shown that modelling and observations are in agreements and hence the contributing noise sources are within the Fresnel zone. Based on the above error analysis it is concluded that errors are in the order of hundredths of seconds, while the signal of interest differ in the order of tenths of seconds.

In conclusion, interferometry applied to pairs or arrays of hydrophones can resolve the deep ocean dispersion over long ranges. Future studies will focus on further use of the dispersive noise field in retrieving deep ocean temperatures and the temperature variations as a function of time. Actual observations of deep ocean temperature changes are of interest, since the deep oceans have shown to take up atmospheric heat over the past fifteen years (see e.g. Balmaseda *et al.* 2013; Chen & Tung 2014).

Future studies will concentrate in applying the method to other array stations, also at other latitudes. It should be noted that the SOFAR channel surfaces close to the poles, making the application of the described methodology challenging.

ACKNOWLEDGEMENTS

The CTBTO and station operators are thanked for the high quality of the IMS data and products. The hydroacoustic data used in this study are available from the virtual Data Exploitation Centre (vDEC) at: http://ctbto.org/specials/vdec/. LE's contribution is partly funded through a VIDI project from the Dutch Science Foundation (NWO), project number 864.14.005. Figures in this paper were made with the Generic Mapping Tools (Wessel & Smith 1991).

REFERENCES

Ball, J.S., Godin, O.A., Evers, L.G. & Lv, C., 2016. Long-range correlations of microseism-band pressure fluctuations in the ocean, *Geophys. J. Int.,* **206,** 825–834.

Balmaseda, M.A., Trenberth, K.E. & Källén, E., 2013. Distinctive climate signals in reanalysis of global ocean heat content, *Geophys. Res. Lett.,* **40,** 1754–1759.

Brown, M.G., Godin, O.A., Williams, N.J., Zabotin, N.A., Zabotina, L. & Banker, G.J., 2014. Acoustic Green's function extraction from ambient noise in a coastal ocean environment, *Geophys. Res. Lett.,* **41,** 5555–5562.

Chapp, E., Bohnenstiel, D.R. & Tolstoy, M., 2005. Sound-channel observations of ice-generated tremor in the Indian Ocean, *Geochem. Geophys. Geosyst.,* **6,** Q06003, doi:10.1029/2004GC000889.

Chen, X. & Tung, K.K., 2014. Varying planetary heat sink led to global-warming slowdown and acceleration, *Science,* **345,** 897–903.

Collins, M.D., 1993. A split-step Padé solution for the parabolic equation method, *J. acoust. Soc. Am.,* **93,** 1736–1742.

Dahlman, O., Mykkeltveit, S. & Haak, H., 2009. *Nuclear Test Ban,* Springer.

De Groot-Hedlin, C., Blackman, D.K. & Jenkins, C.S., 2009. Effects of variability associated with the Antarctic circumpolar current on sound propagation in the ocean, *Geophys. J. Int.,* **176,** 478–490.

De Groot-Hedlin, C.D., 2005. Estimation of the rupture length and velocity of the Great Sumatra earthquake of Dec 26, 2004 using hydroacoustic signals, *Geophys. Res. Lett.,* **32,** L11303, doi:10.1029/2005GL022695.

Dushaw, B.D. *et al.*, 2009. A decade of acoustic thermometry in the North Pacific Ocean, *J. geophys. Res.,* **114,** C07021, doi:10.1029/2008JC005124.

Evers, L.G. & Snellen, M., 2015. Passive probing of the sound fixing and ranging channel with hydro-acoustic observations from ridge earthquakes, *J. acoust. Soc. Am.,* **137,** 2124–2136.

Evers, L.G., Green, D.N., Young, N.W. & Snellen, M., 2013. Remote hydroacoustic sensing of large icebergs in the southern Indian Ocean: implications for iceberg monitoring, *Geophys. Res. Lett.,* **40,** 4694–4699.

Evers, L.G., Brown, D., Heaney, K.D., Assink, J.D., Smets, P.S.M. & Snellen, M., 2014. Evanescent wave coupling in a geophysical system: airborne acoustic signals from the mw 8.1 Macquarie Ridge earthquake, *Geophys. Res. Lett.,* **41,** 1644–1650.

Green, D.N., Evers, L.G., Fee, D., Matoza, R.S., Snellen, M., Smets, P. & Simons, D., 2013. Hydroacoustic, infrasonic and seismic monitoring of the submarine eruptive activity and sub-aerial plume generation at South Sarigan, May 2010, *J. Volcanol. Geotherm. Res.,* **257,** 31–43.

Guilbert, J., Vergoz, J., Schisselé, E., Roueff, A. & Cansi, Y., 2005. Use of hydroacoustic and seismic arrays to observe rupture propagation and source extent of the Mw = 9.0 Sumatra earthquake, *Geophys. Res. Lett.,* **32,** L15310, doi:10.1029/2005GL022966.

Jensen, F.B., Kuperman, W.A., Porter, M.B. & Schmidt, H., 2000. *Computational Ocean Acoustics,* Springer.

Locarnini, R.A., Mishonov, A.V., Antonov, J.I., Boyer, T.P., Garcia, H.E., Baranova, O.K., Zweng, M.M. & Johnson, D.R., 2010. *World Ocean Atlas 2009, Volume 1: Temperature,* NOAA Atlas NESDIS 68, U.S. Government Printing Office, Washington, D.C.

Li, B. & Gavrilov, A., 2009. The significance of horizontal refraction effect for back-azimuth estimation from the CTBT hydroacoustic stations, in *Proceedings of International Scientific Studies Conference,* Vienna, Austria.

Munk, W.H. & Forbes, A.M.G., 1989. Global ocean warming: an acoustic measure?, *J. Phys. Oceanogr.,* **19,** 1765–1777.

Nakata, N., Boué, P., Brenguier, F., Roux, P., Ferrazzini, V. & Campillo, M., 2016. Body and surface wave reconstruction from seismic noise correlations between arrays at Piton de la Fournaise volcano, *Geophys. Res. Lett.,* **43,** 1074–1054.

Prior, M.K., Meless, O., Bittner, P. & Sugioka, H., 2011. Long-range detection and location of shallow underwater explosions using deep-sound-channel hydrophones, *IEEE J. Ocean. Eng.,* **36,** 703–715.

Prior, M.K., Brown, D.J., Haralabus, G. & Stanley, J., 2012. Long-term monitoring of ambient noise at CTBTO hydrophone stations, in *Proceedings of the Underwater Acoustic Measurements Conference,* Edinburgh, UK.

Rickett, J. & Claerbout, J., 1999. Acoustic daylight imaging via spectral factorization: helioseismology and reservoir monitoring, *Leading Edge,* **18,** 957–960.

Roux, P., Kuperman, W.A. & the NPAL Group 2004. Extracting coherent wave fronts from acoustic ambient noise in the ocean, *J. acoust. Soc. Am.,* **116,** 1995–2003.

Sabra, K.G., Fried, S., Kuperman, W.A. & Prior, M., 2012. On the coherent components of low-frequency ambient noise in the Indian Ocean, *J. acoust. Soc. Am.,* **133,** EL20–EL25.

Snieder, R., 2004. Extracting the Green's function from the correlation of coda waves: a derivation based on stationary phase, *Phys. Rev. E,* **69,** doi:10.1103/PhysRevE.69.046610.

Snieder, R. & Wapenaar, K., 2010. Imaging with ambient noise, *Phys. Today,* **63,** 44–49.

Takagi, R. *et al.*, 2015. A single bit matters: coherent noise of seismic data loggers, *Seismol. Res. Lett.,* **86,** 901–907.

Talandier, J., Hyvernaud, O., Reymond, D. & Okal, E.A., 2006. Acoustic signals generated by parked and drifting icebergs in the Southern Indian and Pacific Oceans, *Geophys. J. Int.,* **165,** 817–834.

Wapenaar, K., 2003. Synthesis of an inhomogeneous medium from its acoustic transmission response, *Geophysics,* **68,** 1756–1759.

Weaver, R.L. & Lobkis, O.I., 2001. Ultrasonics without a source: thermal fluctuation correlations at MHz frequencies, *Phys. Rev. Lett.,* **87,** doi:10.1103/PhysRevLett.87.134301.

Wessel, P. & Smith, W.H.F., 1991. Free software helps map and display data, *EOS, Trans. Am. geophys. Un.,* **72,** 441.

Woolfe, K.F. & Sabra, K.G., 2015. Variability of the coherent arrivals extracted from low-frequency deep-ocean ambient noise correlations, *J. acoust. Soc. Am.,* **138,** 521–532.

Woolfe, K.F., Lani, S., Sabra, K.G. & Kuperman, W.A., 2015. Monitoring deep-ocean temperatures using acoustic ambient noise, *Geophys. Res. Lett.,* **42,** 2878–2884.

SUPPORTING INFORMATION

Supplementary data are available at *GJIRAS* online.

Figure S1. The cross correlation coefficient as a function of time for a lag time of 0 s.

Figure S2. Histogram of the velocity over the array for H10N (a) and H10S (b). The velocities are derived from the analysis of over 4000 earthquakes recorded at both arrays.

Please note: Oxford University Press is not responsible for the content or functionality of any supporting materials supplied by the authors. Any queries (other than missing material) should be directed to the corresponding author for the paper.